Gastrointestinal Tumors

ARTICLE

Open Access

https://doi.org/10.48130/git-0026-0011

Gastrointestinal Tumors **2026**, 13: e012

Identification of candidate hub genes and signatures in gastric adenocarcinoma: the role of *CDRT15P1* in tumor progression

Xiao Yang[1#], Kaiyuan Deng[1#], Fengning Wang[2#], Qiao Liu[2], Xinyao Du[2], Yujiao Yang[1], Zhihui Yang[1], Mengqi Yang[3], Liping Wang[1], Xin Wang[1], Shumin Lu[1], Linkun Wang[1], Yuang He[2], Xiang Zhao[2], Jiahui Zhang[2], Fei Xu[2*] and Jiazeng Xia[1,3*]

[1] *Department of General Surgery, Wuxi General Surgery Institute, Jiangnan University Medical Center (Wuxi No.2 People's Hospital), Jiangnan University, Wuxi 214002, China*
[2] *Department of Basic Medicine, Wuxi School of Medicine, Jiangnan University, Wuxi 214122, China*
[3] *Department of General Surgery, The Affiliated Wuxi No.2 People's Hospital of Nanjing Medical University, Wuxi 214002, China*
[#] Authors contributed equally: Xiao Yang, Kaiyuan Deng, Fengning Wang
* Correspondence: xufei@jiangnan.edu.cn (Xu F); xjz_wuxi@alumni.sjtu.edu.cn (Xia J)

Abstract

Gastric cancer (GC) is an aggressive malignancy associated with poor clinical outcomes and continues to impose a substantial global health burden. The present study sought to identify potential hub genes and signatures relevant to clinical outcomes in stomach adenocarcinoma (STAD). Gene expression profiles of gastric tumor tissues and adjacent normal tissues were retrieved from The Cancer Genome Atlas database. Differentially expressed genes (DEGs) shared between tumor and normal tissues were determined by integrating DEG analysis with key gene modules identified through weighted gene co-expression network analysis. Functional enrichment analysis suggested that these genes were primarily associated with proteasome-mediated pathways involved in protein folding, sorting, and degradation. Subsequent Kyoto Encyclopedia of Genes and Genomes pathway analysis combined with machine learning-based feature selection further prioritized candidate hub genes. Five genes—*CDRT15P1*, *LYSMD2*, *STRC*, *KCTD19*, and *ETV2*—were ultimately selected as potential hub genes. To explore possible regulatory associations, transcription factor and miRNA interaction networks were analyzed, together with immune infiltration and tumor-related pathway assessments. *In vitro* functional assays were subsequently conducted to evaluate the effects of *CDRT15P1* knockdown on cell proliferation, migration, invasion, and apoptosis. Overall, the findings indicate that the expression of *CDRT15P1* is associated with biological characteristics related to GC's progression and may have potential relevance in STAD, although further validation is warranted.

Keywords: Gastric cancer, Stomach adenocarcinoma, *CDRT15P1*, Prognosis

Citation: Yang X, Deng K, Wang F, Liu Q, Du X, et al. 2026. Identification of candidate hub genes and signatures in gastric adenocarcinoma: the role of *CDRT15P1* in tumor progression. *Gastrointestinal Tumors* 13: e012 https://doi.org/10.48130/git-0026-0011

Introduction

Gastric cancer (GC) is among the most prevalent malignant tumors globally, ranking fifth in newly diagnosed cancers and fourth in cancer-related mortality[1]. Most patients with GC are not identified until the disease has progressed to an advanced stage, which is associated with unfavorable clinical outcomes[2]. Although studies have shown a steady decline in the incidence of GC in recent years[3], research output related to GC is expected to remain substantial in the foreseeable future. Previous studies have suggested that the development of GC involves multiple biological mechanisms, including DNA damage repair and chronic inflammation of the gastric epithelium[4–8]. GC represents the final outcome of long-term pathological processes involving the accumulation of multiple genetic and epigenetic alterations. Although numerous genes have been reported to be involved in GC-related progression and clinical outcomes[9,10], effective molecular targets for predicting GC remain to be identified.

Weighted correlation network analysis (WGCNA) is a widely used bioinformatics approach for exploring gene expression patterns across different samples; it groups genes with comparable expression profiles into modules, enables the analysis of relationships between modules and specific traits or phenotypes, and facilitates the identification of intramodular hub genes[11,12]. Least absolute shrinkage and selection operator (LASSO) regression is a regularization-based estimation method that extends the least squares approach, aiming to achieve an optimal balance between a model's simplicity and predictive accuracy. In this study, hub genes associated with stomach adenocarcinoma (STAD) were identified through integrated bioinformatics analyses combined with machine learning algorithms and LASSO regression.

CMT1A replication region transcript 15 (*CDRT15*) was initially described by Inoue et al. in 2001 during investigations of the 1.4-Mb genomic region associated with *Charcot–Marie–Tooth disease Type 1A* (*CMT1A*) duplication and *hereditary neuropathy with liability to pressure palsy* (*HNPP*) deletion[13]. According to current genome annotations (GRCh38/hg38), *CDRT15* is located on chromosome 17 (17:14,235,673–14,236,862) and spans 1,190 nucleotides. The encoded product is referred to as the CDRT15 protein. Previous studies have reported elevated expression of CDRT15 in cholangiocarcinoma (CCA)[14], where higher expression levels were associated with unfavorable clinical outcomes and alterations in immune cell infiltration patterns. These findings suggest that CDRT15 may have potential clinical relevance as a biomarker in CCA. However, its involvement in GC has not been clearly characterized. Subsequent research has indicated that *CDRT15*-related transcripts may participate in various biological processes across different physiological and pathological contexts, particularly in malignant diseases. In light of these observations, we examined the expression pattern of *CDRT15 pseudogene 1*(*CDRT15P1*) in GC using The Cancer Genome Atlas (TCGA) datasets and evaluated its relationship with clinicopathological features. In addition, *in vitro* functional assays were

https://doi.org/10.48130/git-0026-0011

conducted to assess the potential association between the expression of *CDRT15P1* and phenotypic behaviors of GC cells.

Materials and methods

Data source and preprocessing

Transcriptomic profiles of STAD and the corresponding adjacent non-tumor tissues were retrieved from TCGA repository. Only samples with complete expression information were included, comprising 32 normal tissue specimens and 375 GC tissue specimens. The adjacent normal tissues were derived from the gastric mucosa of the same patients and were collected from noncancerous regions more than 2 cm away from the tumor margin. To minimize technical variability across samples, transcript abundance values were transformed using $\log_2$ (transcripts per million [TPM] + 1) prior to downstream analyses[15].

Construction of the gene co-expression network

To investigate coordinated transcriptional patterns associated with STAD, a weighted gene co-expression framework was established using normalized RNA sequencing data. Genes exhibiting greater variability across samples were preferentially selected to enhance the network's robustness. Specifically, genes ranked within the upper 50% of variance and presenting a median absolute deviation (MAD) greater than 0.01 were retained. A range of candidate soft-thresholding parameters was examined, and the value that achieved an approximate scale-free topology while preserving adequate network connectivity was selected for adjacency calculation. Pairwise gene correlations were converted into connection strengths and further transformed into topological overlap measures to characterize shared neighborhood similarity. Hierarchical clustering based on topological overlap dissimilarity was subsequently performed to group genes with similar expression patterns. Modules were identified through dynamic branch segmentation, and modules displaying high similarity were consolidated according to a predefined merging threshold.

Identification of candidate hub genes

To reduce redundancy among genes and improve the model's interpretability, a penalized regression approach was adopted for variable selection. LASSO regression was implemented using the "glmnet" package in R. Model tuning was conducted through 10-fold cross-validation, and the penalty coefficient corresponding to the minimum cross-validation error was selected. Genes retained at this optimal parameter were considered to be potential hub candidates.

Differential expression analysis

Differential gene expression between tumor and adjacent normal tissues was evaluated using R statistical software. After normalization, genes meeting the criteria of an absolute $\log_2$ fold change greater than 1.5 and an adjusted *p*-value below 0.05 were regarded as significantly dysregulated.

Construction of regulatory networks of transcription factors and miRNAs

We identified the pre- and post-transcriptional gene regulatory factors of microRNA (miRNA) and the transcriptional factors (TFs) by analyzing the interaction networks among the shared hub genes' encoded proteins and miRNAs and TFs. The interaction network of TFs and shared differentially expressed hub genes (hub-DEGs) was constructed using the JASPAR[16] TF database, and the TarBase V8.0[17] and miRTarBase[18] miRNAs databases were utilized to construct the miRNA–hub-DEG interaction network.

Immune infiltration estimation

To characterize the immune landscape of STAD samples, enrichment scores representing immune cell populations were computed at the individual sample level using a single-sample gene set enrichment framework. Associations between hub genes' expression and immune infiltration scores were assessed by correlation analysis[19].

Cell culture conditions

The human gastric carcinoma cell lines AGS and MKN-45 were obtained from the Cell Resource Center of the Chinese Academy of Medical Sciences (Beijing, China). AGS cells were maintained in Dulbecco's modified Eagle medium (DMEM), whereas MKN-45 cells were cultured in Roswell Park Memorial Institute (RPMI)-1640 medium. Both media were supplemented with 10% fetal bovine serum and standard concentrations of penicillin (100 U/mL) and streptomycin (100 μg/mL). Cells were incubated at 37 °C under 5% CO_2 in a humidified atmosphere. The culture medium was replaced every 48 h to maintain optimal growth conditions. All *in vitro* experiments were independently repeated three times, with three technical replicates per experiment.

Gene silencing procedure

To assess the biological role of *CDRT15P1*, transient knockdown experiments were performed using small interfering RNA (siRNA). Transfections were carried out according to the manufacturer's protocol provided with the siRNA transfection kit. Following transfection, cells were incubated for 48 h before the subsequent analyses. Knockdown efficiency was confirmed by quantitative real-time polymerase chain reaction (qRT-PCR). Cells transfected with a non-targeting siRNA sequence served as the negative controls. The siRNA sequences and qRT-PCR primer sequences are listed in Supplementary Table S1.

Quantitative real-time polymerase chain reaction

Total RNA was isolated using TRIzol reagent following standard extraction procedures. One microgram of total RNA was reverse-transcribed into complementary DNA using a commercial synthesis kit. Real-time polymerase chain reaction (PCR) amplification was conducted using SYBR Green chemistry. Relative gene expression levels were calculated using the $2^{-\Delta\Delta Ct}$ method, with appropriate internal controls applied for normalization.

Protein expression analysis

Whole-cell protein lysates were prepared using Radio Immunoprecipitation Assay (RIPA) buffer supplemented with protease inhibitors. Protein concentrations were quantified using a bicinchoninic acid (BCA) assay. Equal amounts of protein were separated via sodium dodecyl sulfate–polyacrylamide gel electrophoresis (SDS-PAGE) and transferred onto polyvinylidene difluoride (PVDF) membranes. After blocking, the membranes were incubated overnight at 4 °C with primary antibodies targeting Phosphatidylinositol 3-kinase (PI3K), phosphorylated PI3K, AKT serine/threonine kinase (also known as Protein Kinase B, PKB), phosphorylated AKT, and

β-actin. Subsequently, membranes were exposed to horseradish peroxidase-conjugated secondary antibodies. Immunoreactive bands were detected using enhanced chemiluminescence reagents.

Assessment of cell proliferation

Cell viability was evaluated using the cell counting kit-8 (CCK-8) assay. Transfected cells were seeded into 96-well plates at a density of 3×10^3 cells per well. At 24, 48, 72, and 96 h post-seeding, CCK-8 reagent was added according to the manufacturer's instructions. Optical density values were measured at 450 nm to estimate proliferative capacity.

Migration analysis

To examine migratory behavior, wound-healing assays were performed. Cells were cultured in six-well plates until reaching near-complete confluence. A sterile pipette tip was used to generate a linear scratch across the monolayer. After washing away detached cells, cultures were maintained in serum-free medium. Images were captured at predefined time points to monitor the wound closure dynamics.

Invasion assay

Cell invasive potential was evaluated using transwell chambers coated with Matrigel. Transfected cells were suspended in serum-reduced medium and placed in the upper chamber. The lower chamber contained the medium supplemented with 10% fetal bovine serum as a chemoattractant. Following incubation, noninvading cells were removed from the upper surface of the membrane. Cells that traversed the membrane were fixed, stained with crystal violet, and quantified microscopically.

Apoptosis analysis

Apoptotic populations were analyzed using Annexin V-fluorescein isothiocyanate (FITC)/propidium iodide dual staining. Cells were harvested 48 h after transfection, washed with phosphate-buffered saline, and resuspended in binding buffer. Staining reagents were applied sequentially according to the manufacturer's instructions. Flow cytometry was used to distinguish the early and late apoptotic fractions.

Statistical considerations

All analyses were conducted using R software (version 3.6.1) and GraphPad Prism (version 9.5.1). Comparisons between two groups were performed using Student's *t*-test. For multiple-group comparisons, one-way analysis of variance (ANOVA) was applied. The Benjamini–Hochberg method was applied for multiple testing correction in the enrichment analysis and all correlation analyses to control the false discovery rate (FDR). Statistical significance was defined as a two-sided *p*-value less than 0.05.

Results

WGCNA analysis and identification of key modules

Differential expression analysis between tumor and adjacent normal gastric tissues yielded 20,525 genes meeting the predefined screening criteria (adjusted $p < 0.05$ and $|\log_2$ fold change$| > 1.5$). Among these, 10,501 genes showed increased expression, whereas 10,024 exhibited decreased expression in STAD samples. The expression distribution profile is summarized in Fig. 1a.

To further investigate coordinated transcriptional behavior, a co-expression network was constructed using the filtered dataset. When multiple probes mapped to the same gene symbol, the probe with the highest average expression value was selected to represent that gene. Genes demonstrating relatively higher variability across samples (top 50% based on MAD and MAD > 0.01) were retained for network modeling.

Evaluation of the candidate soft-thresholding parameters indicated that $\beta = 6$ provided a satisfactory approximation of scale-free topology ($R^2 = 0.85$; Fig. 1b). This parameter was therefore used to compute pairwise gene connectivity, which was subsequently converted into topological overlap measures to better capture shared interaction patterns. Modules were defined using hierarchical clustering, with a minimum size of 30 genes. Modules exhibiting high similarity (correlation > 0.75) were merged to reduce redundancy.

Correlation analysis between module eigengenes and clinical traits identified several modules strongly associated with STAD status (Fig. 1c). The magenta ($r = -0.86$, $p = 2E{-}47$), green ($r = -0.74$, $p = 6E{-}29$), cyan ($r = -0.69$, $p = 1E{-}23$), and purple ($r = -0.69$, $p = 1E{-}23$) modules demonstrated the most pronounced relationships and were therefore prioritized for downstream investigation.

The clustering dendrogram and corresponding module color annotations are displayed in Fig. 1e. The heatmap in Fig. 1d illustrates gene–gene connectivity patterns within the network. Furthermore, associations between gene significance and module membership were examined within the selected modules, revealing strong correlations in the magenta, green, and cyan modules, and a moderate association in the purple module (Fig. 1f–i).

Screening of hub genes

To further refine candidate genes derived from the overlapping differentially expressed gene (DEG) set, LASSO regression analysis was performed to minimize model overfitting and identify the most informative variables (Fig. 2a, b). The optimal penalty parameter (λ) was determined by 10-fold cross-validation. At $\lambda = 0.01$, five genes—*CDRT15P1*, *LYSMD2*, *STRC*, *KCTD19*, and *ETV2*—were retained for subsequent analyses.

Univariate Cox proportional hazards regression was then conducted to evaluate their prognostic significance. Four genes were identified as risk-associated factors, whereas one gene exhibited a protective effect (Fig. 2c, d).

For survival analysis, patients were stratified into high- and low-expression groups according to optimal cut-off values. The corresponding thresholds were 0.002 for *CDRT15P1*, 0.001 for *LYSMD2*, 0.001 for *STRC*, 0.002 for *KCTD19*, and 0.001 for *ETV2*.

Kaplan–Meier survival curves demonstrated that elevated expression of *CDRT15P1* ($p = 0.002$) and *KCTD19* ($p = 0.029$) was significantly associated with poorer overall survival, whereas higher *ETV2* expression ($p = 0.009$) was associated with favorable survival outcomes (Fig. 2e). No statistically significant differences were observed for the remaining genes.

Functional enrichment analysis of common DEGs in normal and STAD tissues

To characterize the biological functions potentially associated with the overlapping DEGs identified in STAD, pathway enrichment analysis was conducted using the Kyoto Encyclopedia of Genes and

https://doi.org/10.48130/git-0026-0011

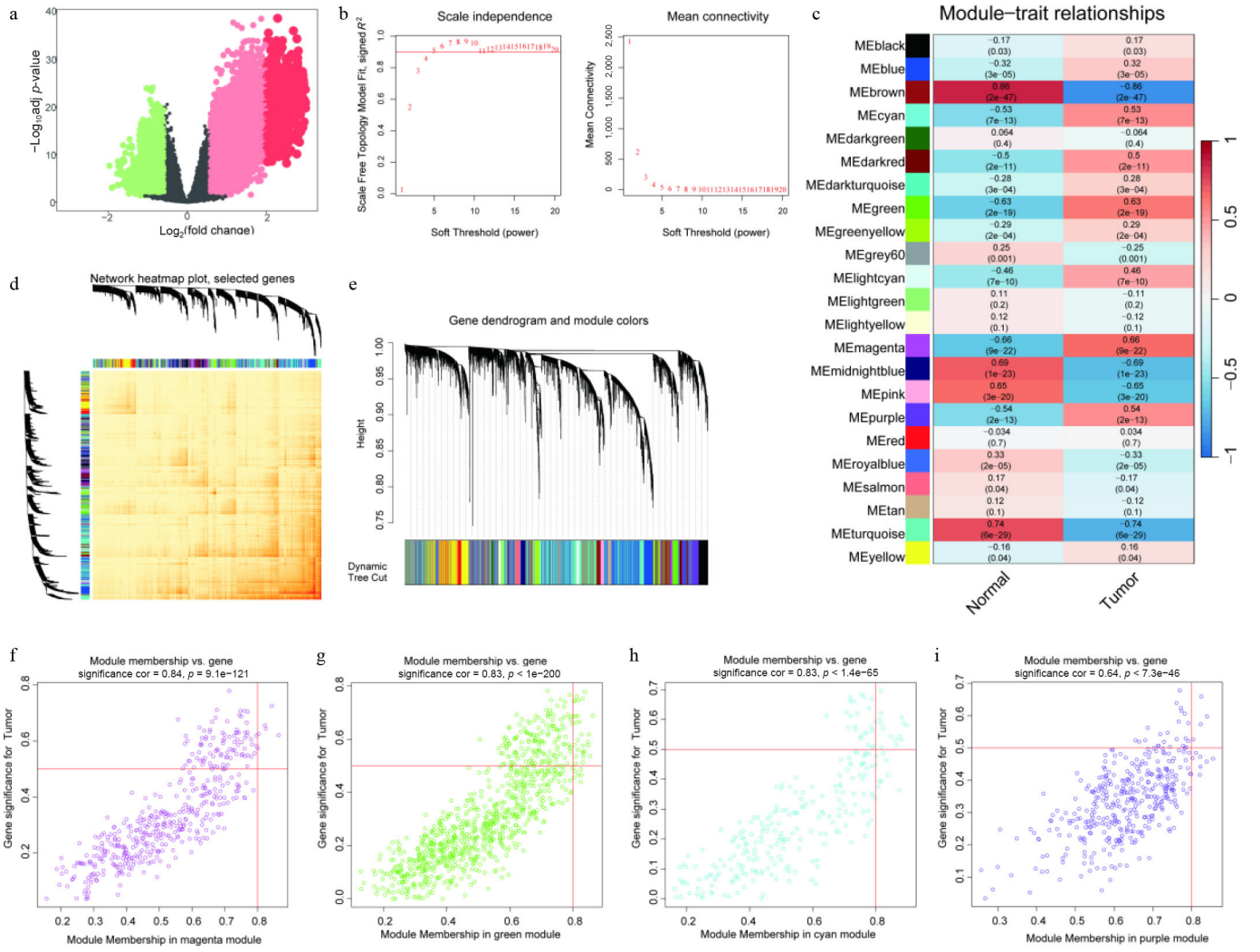

Fig. 1 Differential expression and co-expression network analysis in STAD. (a) Distribution of differentially expressed genes (DEGs) between tumor and normal gastric tissues visualized by a volcano plot. (b) Determination of the soft-thresholding power ($\beta = 6$) based on the scale-free topology fit and mean connectivity analysis. (c) Correlation matrix illustrating the relationships between gene modules and STAD clinical traits. (d) Topological overlap matrix heatmap showing gene connectivity patterns. (e) Hierarchical clustering dendrogram with module color assignment. (f)–(i) Correlation analysis between module membership and gene significance for the magenta, green, cyan, and purple modules.

Genomes (KEGG) database. The enrichment profile indicated that metabolic pathways constituted the predominant functional category among these genes. In particular, the pathway related to metabolism of cofactors and vitamins exhibited the highest level of statistical significance (Fig. 3). In addition to metabolic processes, genes involved in proteasome-mediated protein folding, sorting, and degradation were also enriched (Fig. 3). These findings suggest that alterations in metabolic regulation and protein processing may be linked to the molecular characteristics of STAD, although further experimental validation is required to clarify their precise biological implications.

Correlation analysis between hub gene expression and tumor-related biological pathways

We next examined the associations between hub genes' expression levels and tumor-related biological features. Elevated *CDRT15P1* expression showed positive correlations with proliferation ($R = 0.16$, $p = 0.00084$), stemness ($R = 0.20$, $p = 6.3e{-}05$), and differentiation ($R = 0.18$, $p = 2e{-}04$) scores (Fig. 4a). These correlations suggest a potential relationship between *CDRT15P1*'s expression and phenotypic characteristics associated with tumor progression, although the strength of these associations was modest. A comparable pattern was observed for *KCTD19*, which displayed positive correlations with angiogenesis ($R = 0.15$, $p = 0.0016$) and apoptosis ($R = 0.13$, $p = 0.0075$) (Fig. 4c). In contrast, *ETV2*'s expression demonstrated a different correlation profile. *ETV2* was positively associated with quiescence ($R = 0.19$, $p = 7.6e{-}05$) but showed negative correlations with angiogenesis ($R = -0.28$, $p = 1.1e{-}08$), differentiation ($R = -0.27$, $p = 1.9e{-}08$), and epithelial–mesenchymal transition (EMT) ($R = -0.24$, $p = 1e{-}06$) (Fig. 4b). In addition, *ETV2*'s expression was negatively correlated with invasion ($R = -0.18$, $p = 0.00031$) and metastasis ($R = -0.22$, $p = 5.6e{-}06$), suggesting that higher *ETV2* levels may be associated with comparatively less aggressive phenotypic features. Consistent with these observations, the expression of *ETV2* was lower in STAD tissues compared with normal tissues (Fig. 2e), and reduced *ETV2* expression was associated with improved overall survival in STAD patients (Fig. 2e). By contrast, the opposite trends were observed for *CDRT15P1* and *KCTD19*.

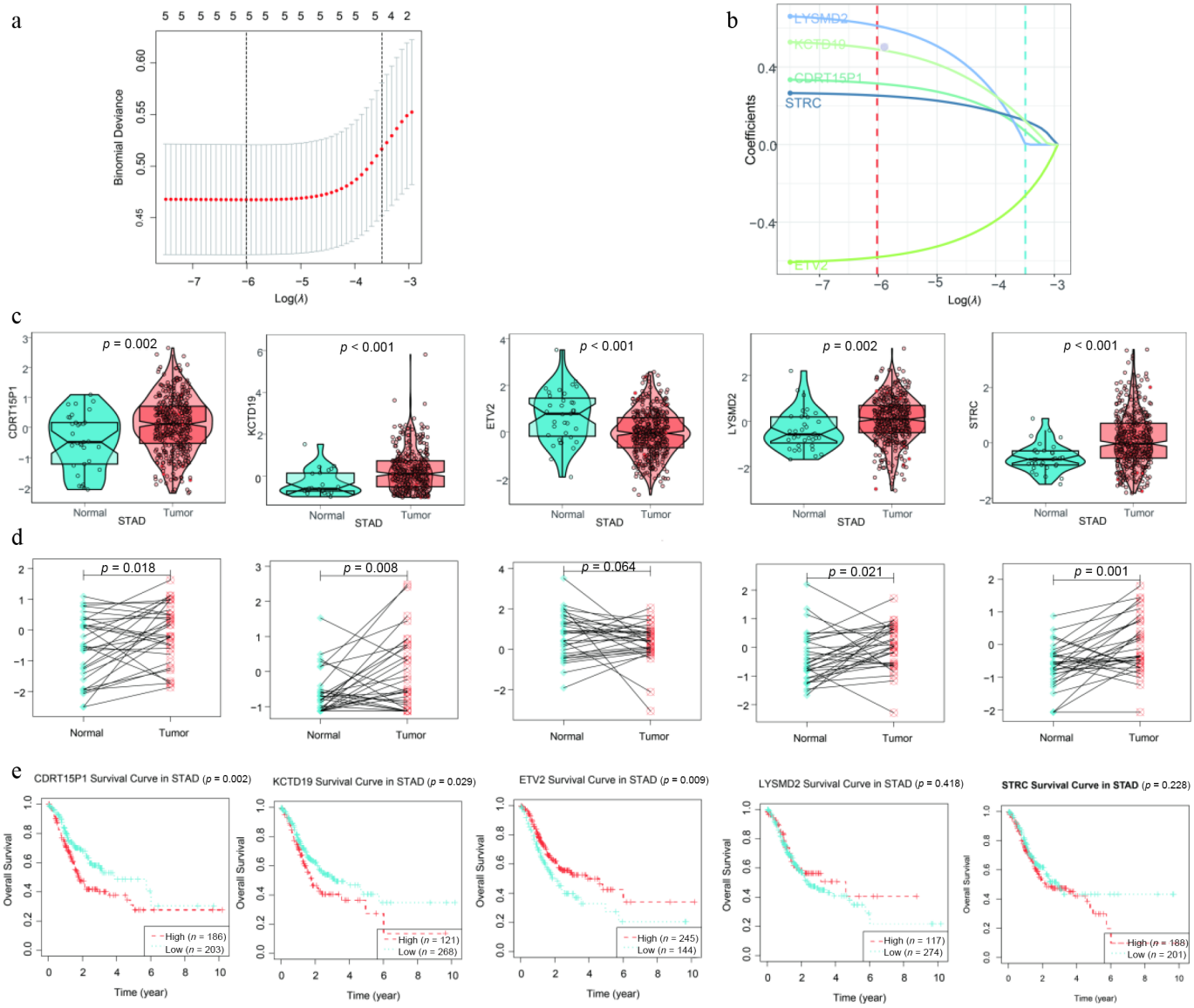

Fig. 2 Identification and prognostic evaluation of hub genes. (a), (b) Construction of the LASSO regression model and selection of the optimal λ value using cross-validation. (c), (d) Comparison of gene expression levels between tumor and normal tissues. (e) Kaplan–Meier survival analysis stratified by the expression levels of selected hub genes in STAD patients.

Furthermore, both *CDRT15P1* and *KCTD19* showed positive correlations with DNA damage repair signatures. These associations raise the possibility that their expression levels may be linked to cellular responses to radiotherapy or chemotherapy; however, this hypothesis requires additional experimental validation.

Association between hub genes and immune cell infiltration

Given the established role of immune cell dynamics in tumor development, we further evaluated the relationship between hub genes' expression and estimated immune cell infiltration in STAD samples. Analysis indicated that the expression of *CDRT15P1* exhibited modest correlations with variations in immune cells' abundance, particularly involving T lymphocytes, B lymphocytes, macrophages, and mast cells (Fig. 5a).

A similar tendency was observed for *KCTD19*, where expression levels were also related to patterns of T cell and B cell infiltration (Fig. 5c).

In contrast, the correlation pattern associated with *ETV2* differed, as its expression showed the opposite tendency with respect to T cell and B cell infiltration (Fig. 5b).

Overall, higher *CDRT15P1* expression appeared to correspond to slightly reduced immune cell infiltration across several immune subsets. However, the magnitude of these correlations was relatively limited, and the findings primarily reflect general trends rather than strong quantitative effects.

Construction of transcriptional regulatory networks

To further explore potential upstream regulatory relationships of the identified hub genes, TF and microRNA interaction analyses were performed.

On the basis of predictive databases, regulatory interactions were mapped and organized into a gene-centered network, which was subsequently displayed using Cytoscape (Fig. 6). The resulting structure included a four-node gene–miRNA interaction framework.

https://doi.org/10.48130/git-0026-0011

Fig. 3 Functional enrichment analysis of overlapping DEGs. Pathway enrichment was performed using publicly available KEGG annotations. Pathway diagrams were generated by the authors on the basis of KEGG database information without direct reproduction of original KEGG images.

Within the TF–hub gene interaction analysis, *CDRT15P1*, *LYSMD2*, and *KCTD19* were associated with a relatively larger number of predicted TFs compared with the remaining genes. Among these TFs, SCRT1 and ZFX appeared more frequently across multiple hub genes. The gene–miRNA interaction mapping indicated that *CDRT15P1*, *KCTD19*, and *LYSMD2* were connected to several predicted miRNAs. Specifically, hsa-miR-26b-5p, hsa-let-7g-5p, hsa-miR-148b-3p, hsa-let-7i-5p, hsa-miR-26a-5p, and hsa-miR-34a-5p were predicted to interact with both *CDRT15P1* and *KCTD19*. In addition, hsa-miR-182-5p, hsa-miR-20b-5p, and hsa-miR-129-2-3p were linked to *LYSMD2* and *KCTD19*.

These analyses provide a preliminary overview of potential regulatory connections, although experimental validation would be required to confirm these predicted interactions.

CDRT15P1 affects the proliferation, migration, invasion, and apoptosis of GC cells *in vitro*

Since *CDRT15P1* is located within the *CMT1A* duplication region on chromosome 17p12, and its gene name is derived from this region, we performed an intersection analysis between the DEGs in STAD and the *CMT1A*-related gene set (Fig. 7a) to evaluate the overall differential expression characteristics of this gene family in GC. The results showed that *CDRT15P1* is one of the most significant DEGs within the *CMT1A*-related gene set. To further investigate the potential biological role of *CDRT15P1* in GC cells, loss-of-function experiments were performed using siRNA-mediated knockdown in AGS and MKN-45 cell lines. qRT-PCR confirmed that *CDRT15P1*'s expression was effectively reduced following siRNA transfection in both cell lines (Fig. 7b). Cell viability was subsequently evaluated using CCK-8 assays at multiple time points. Compared with cells transfected with negative control siRNA, *CDRT15P1*-silenced cells exhibited decreased proliferation rates in both AGS and MKN-45 cells (Fig. 7c). Consistent with these findings, colony formation capacity was also reduced after *CDRT15P1* knockdown (Fig. 7d). To assess cell motility, wound-healing assays were conducted. Cells with reduced *CDRT15P1* expression demonstrated slower wound closure relative to the control cells in both cell lines (Fig. 7e). In parallel, transwell assays indicated that silencing *CDRT15P1* was associated with a reduction in invasive cell numbers (Fig. 7f). Apoptotic cell populations were analyzed by flow cytometry using Annexin V-FITC/propidium iodide staining. An increase in both early and late apoptotic fractions was observed in *CDRT15P1*-knockdown cells compared with the controls (Fig. 7g). To explore potential downstream signaling alterations, the PI3K/AKT pathway was examined by Western blotting. Reduced phosphorylation levels of PI3K and AKT were detected in *CDRT15P1*-silenced cells, whereas total protein levels showed no marked changes (Fig. 7h). Collectively, these results suggest that decreased *CDRT15P1* expression is associated with reduced proliferative and migratory capacities and increased apoptotic tendency in GC cells. However, the precise molecular mechanisms underlying these observations require further investigation.

Discussion

In the past few decades, the incidence rate of GC has declined steadily worldwide[20], mainly because of the successful prevention and treatment of *Helicobacter pylori* infection. The clinical therapy of GC includes surgery, adjuvant chemotherapy, neoadjuvant chemotherapy, and immunotherapy[21–25]. Given that conventional treatment strategies often fail, many cancer-related molecules have been characterized with the aim of developing novel anticancer therapies, including targeted antibodies and vaccines[26]. With the rise of immunotherapy, four main strategies are currently considered: Immune checkpoint inhibitors (ICI), tumor vaccines, adoptive immunotherapy (ACT), and nonspecific immunomodulators[27]. Despite many advances in the therapeutic field, the prognosis and quality of life of GC patients have hardly improved in the past decade[28].

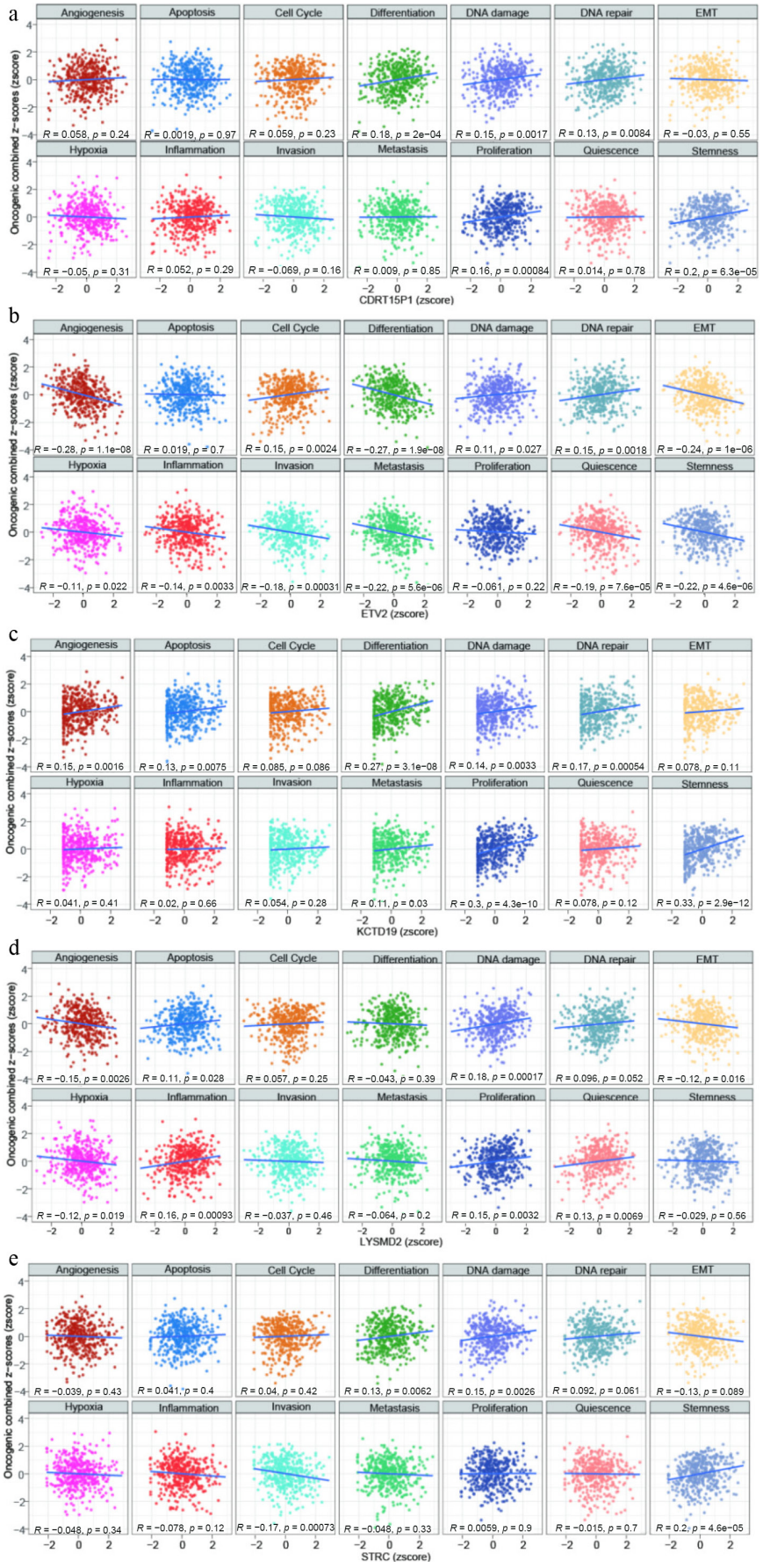

Fig. 4 Correlation between hub genes' expression and tumor-related biological features. (a) *CDRT15P1*; (b) *ETV2*; (c) *KCTD19*; (d) *LYSMD2*; (e) *STRC*. Correlation coefficients and corresponding *p*-values are indicated in each panel.

https://doi.org/10.48130/git-0026-0011

Fig. 5 (continued)

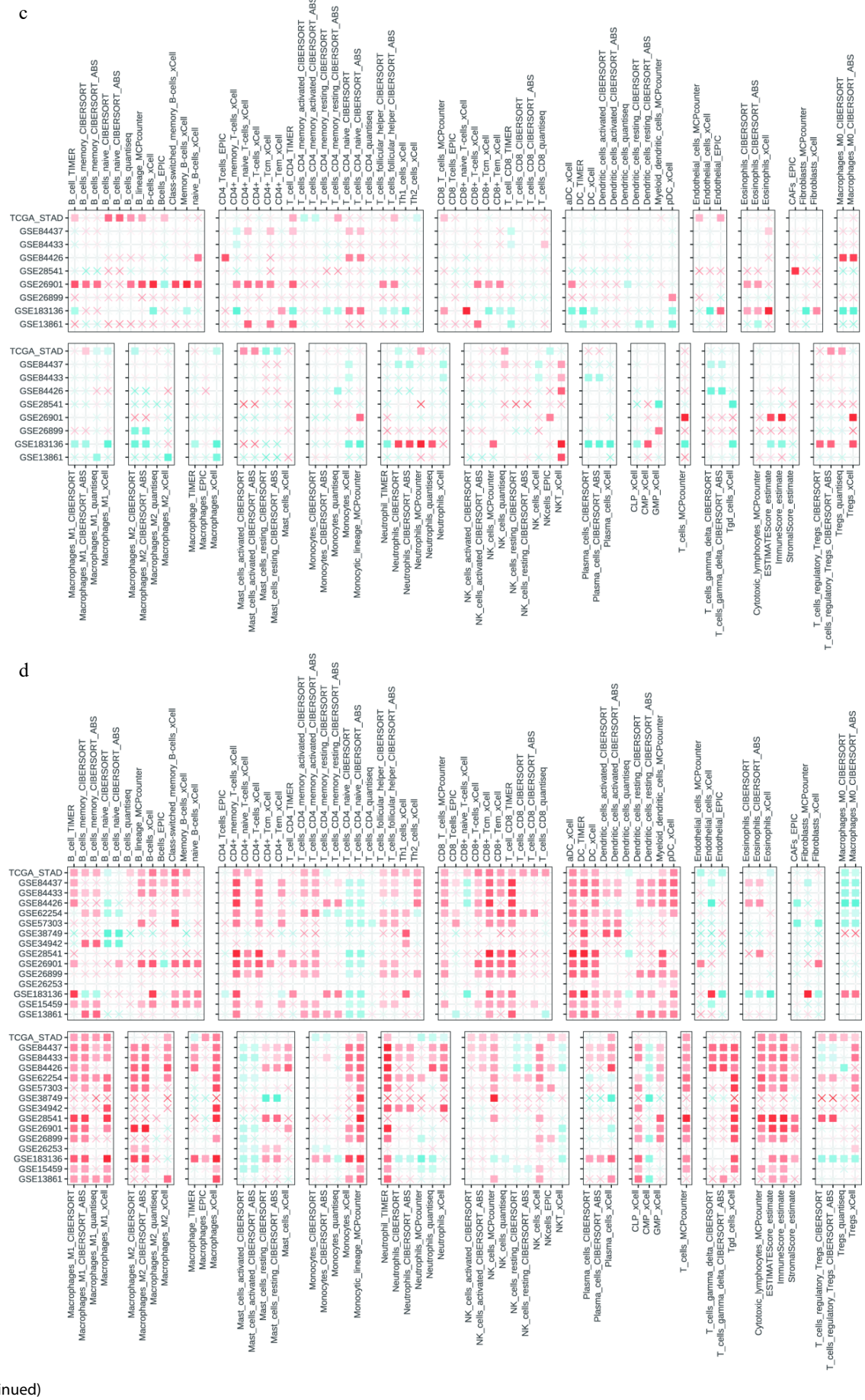

Fig. 5 (continued)

https://doi.org/10.48130/git-0026-0011

Fig. 5 Association between hub genes' expression and immune cell infiltration in STAD. (a) *CDRT15P1*; (b) *ETV2*; (c) *KCTD19*; (d) *LYSMD2*; (e) *STRC*. Immune infiltration scores were estimated using single sample Gene Set Enrichment Analysis (ssGSEA).

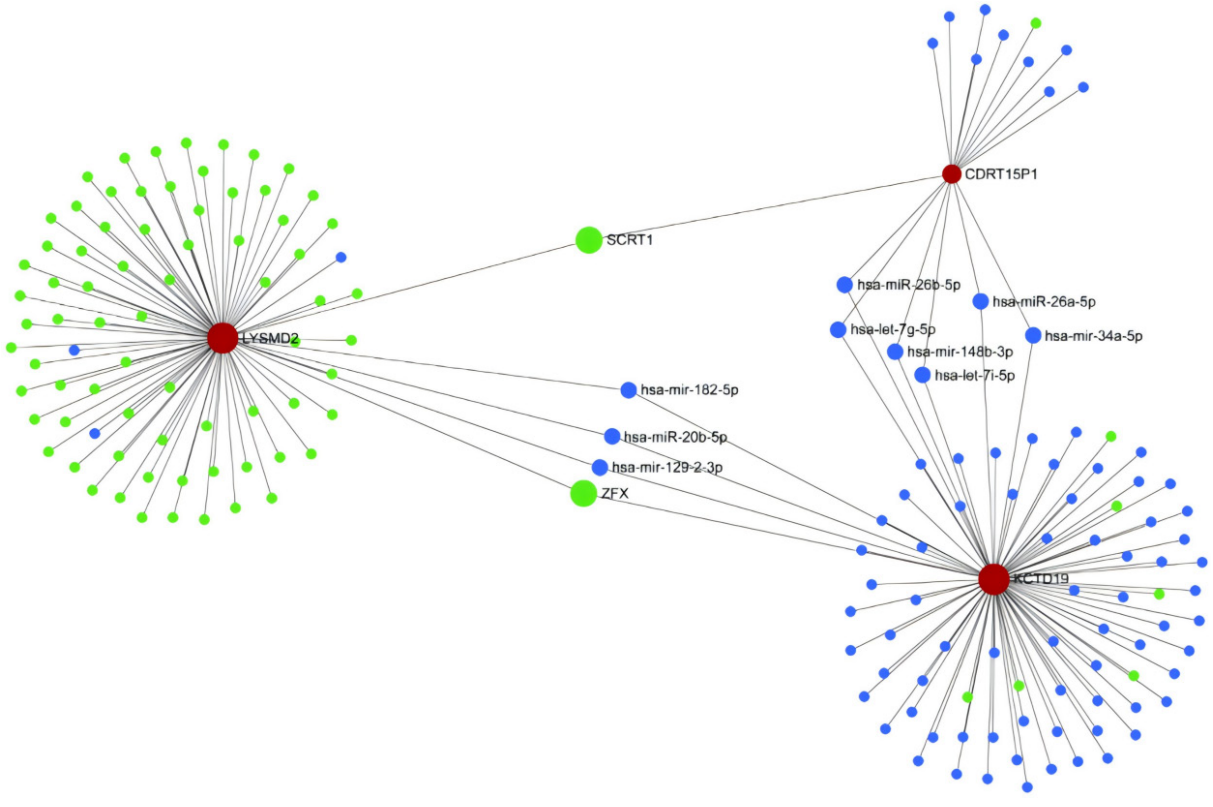

Fig. 6 Predicted transcription factor and miRNA interaction network of STAD-related hub genes. Green nodes represent transcription factors and blue nodes represent miRNAs.

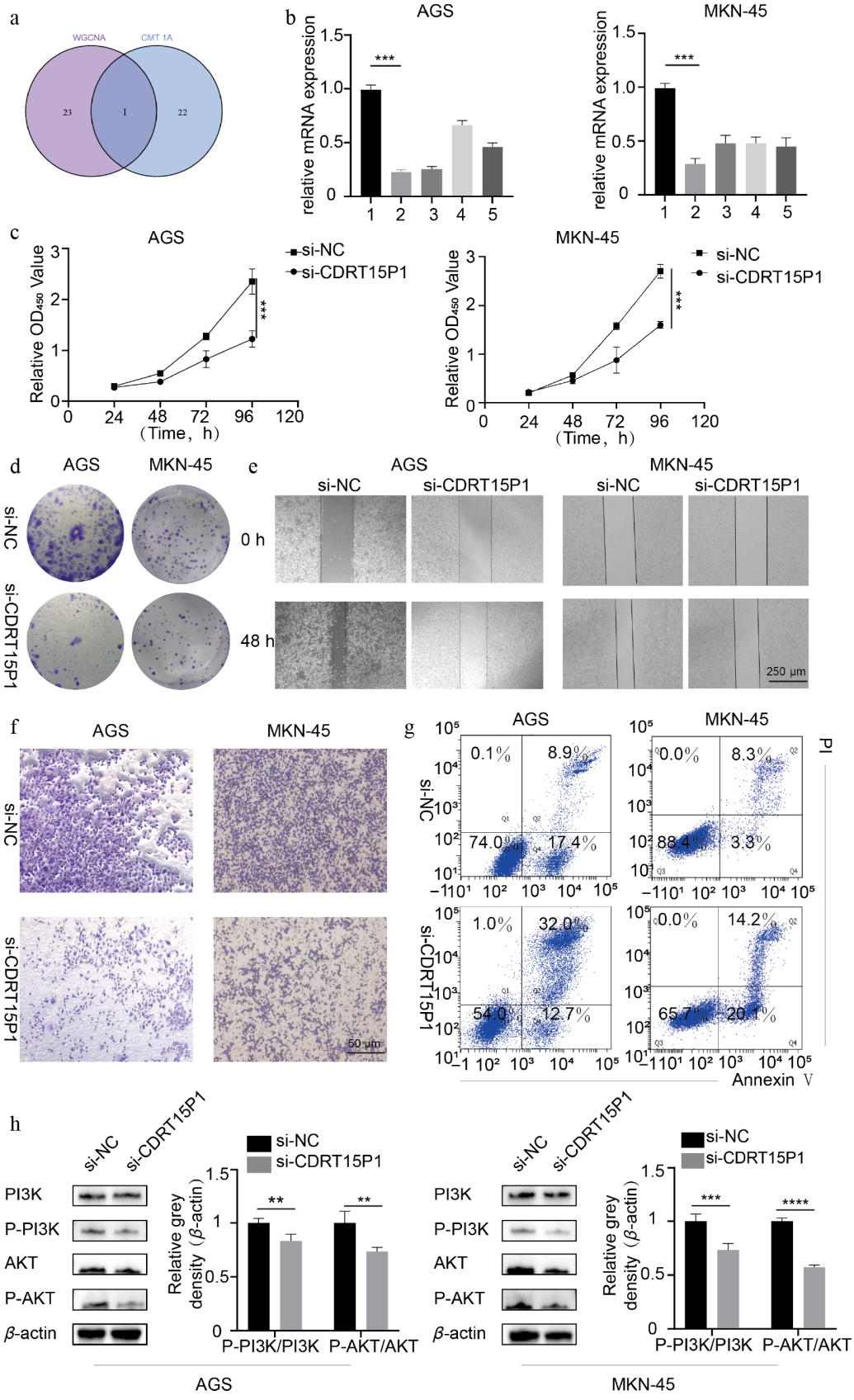

Fig. 7 Functional assessment of *CDRT15P1* in GC cells. (a) Venn diagram showing the overlap between DEGs and *CMT1A*-related gene sets. (b) Relative mRNA expression of *CDRT15P1* following siRNA transfection. (c) Cell proliferation assessed by the CCK-8 assay. (d) Colony formation assay. (e) Wound-healing assay evaluating migratory capacity. (f) Transwell invasion assay. (g) Apoptosis analysis by Annexin V-FITC/propidium iodide staining. (h) Western blot analysis of PI3K/AKT pathway proteins following *CDRT15P1* knockdown. Data are presented as the mean ± SD. * $p < 0.05$, ** $p < 0.01$, *** $p < 0.001$, **** $p < 0.0001$.

https://doi.org/10.48130/git-0026-0011

The 17p12 chromosomal region contains a 1.4-Mb segment flanked by two approximately 24-kb low-copy repeat sequences (CMT1A–REPs). Structural rearrangements within this region have been reported to give rise to inherited peripheral neuropathies, including CMT1A and HNPP. *CDRT15P1* is one of the genes in this genomic region. In the study of Tianyang Yu et al., the results showed that the elevated expression of *CDRT15P1* was associated with a higher incidence rate and poorer prognosis of cholangiocarcinoma. At present, there are no reports on whether *CDRT15P1* has a role in the occurrence and development of GC. We conducted biological information analysis on the TCGA database between normal and tumor tissues of the stomach, and the results showed that *CDRT15P1* expression was increased in tumor tissues. We analyzed the expression level of *CDRT15P1* and its relationship with GC-related cellular function. The results showed that increased expression of *CDRT15P1* was associated with elevated levels of proliferation-related factors, stemness factors, and differentiation factors in GC cells, which suggested a higher risk of metastasis and invasion.

CDRT15P1 expression showed a negative correlation with the infiltration levels of multiple immune cell types in STAD, including T cells, B cells, macrophages, and mast cells. Concurrently, *in vitro* functional assays revealed that CDRT15P1 knockdown significantly reduced PI3K/AKT phosphorylation levels. These two independent observations suggest a potential link between *CDRT15P1* expression, PI3K/AKT pathway activity, and the tumor immune microenvironment. Notably, emerging evidence has linked PI3K/AKT signaling to immune infiltration patterns across various solid tumors. In hepatocellular carcinoma, FAT10 upregulates *PD-L1* expression by activating the PI3K/AKT/mammalian targed of rapamycin (mTOR) pathway, thereby suppressing CD8+ T cell infiltration and promoting immune evasion[29]. Similarly, in the GC microenvironment, interleukin (IL)-4 induces metabolic reprogramming and M2 polarization of macrophages by upregulating the PI3K/AKT/mTOR signaling pathway, leading to CD8+ T cell dysfunction and resistance to anti-PD-1 therapy[30]. Furthermore, SERPINE1 in gastric cancer activates the PI3K/AKT pathway through autocrine mechanisms to promote anoikis resistance, while also promoting M2 macrophage polarization and suppressing CD8+ T cell infiltration and function via paracrine binding to LRP1[31]. In breast cancer, inhibition of the PI3K/AKT pathway has been shown to downregulate *PD-L1* expression in tumor cells, promote macrophage polarization toward the M1 phenotype, enhance CD8+ T cells' function, and increase T and B cells' tumor infiltration[32]. The findings of these studies, in conjunction with our observations, support the reasonable hypothesis that *CDRT15P1* may contribute to shaping an immunosuppressive microenvironment in GC, including inhibiting T cell infiltration and promoting M2 polarization of macrophages, at least in part through activation of the PI3K/AKT pathway. This could partially explain the association between high *CDRT15P1* expression and poor clinical outcomes. Nevertheless, it is important to acknowledge that our study currently provides only indirect, correlational evidence. Whether the *CDRT15P1*/PI3K/AKT axis directly influences immune cell infiltration and through which molecular mediators this occurs (e.g., PD-L1, chemokines) are questions that require direct validation using immune cell–tumor cell co-culture models or *in vivo* xenograft models.

Among the five candidate hub genes, *CDRT15P1* was the only one showing significantly upregulated expression in STAD, a strong association with poor prognosis, and positive correlations with multiple malignant phenotypes (proliferation, stemness, differentiation). Therefore, it was prioritized for further functional investigation. We conducted functional experiments on GC cells *in vitro*, including examinations of proliferation, migration, invasion, and apoptosis. The results showed that increased *CDRT15P1* expression levels promoted the proliferation, migration, and invasion of GC cells, while inhibiting apoptosis. Collectively, these findings suggest that *CDRT15P1* may contribute to GC's progression. Through KEGG enrichment analysis, we found that elevated *CDRT15P1* expression may be associated with alterations in cofactor metabolism pathways. Numerous studies have reported the involvement of cofactor metabolism in GC's progression[33]. Therefore, it is necessary to find the cofactors involved in the regulation of GC by *CDRT15P1*.

However, there are limitations to this study. The small number of GC patients in TCGA and other databases may result in significant bias. Moreover, this study did not collect tissues from specific clinical cases for experimentation. The biological function and mechanism of *CDRT15P1* in GC require further experimental verification. In addition, more robust validation needs to be done to confirm the role of *CDRT15P1* in the prognosis of GC through *in vivo* or *in vitro* studies. A major limitation of this study is the lack of *in vivo* validation. Though our bioinformatics and *in vitro* findings suggest a potential role for *CDRT15P1* in gastric adenocarcinoma, animal model experiments are needed to further confirm its functional significance. We therefore plan to conduct rigorous *in vivo* studies in the future. Whether the PI3K/AKT pathway mediates all observed phenotypes requires further validation through pathway rescue experiments.

Conclusions

In summary, our results demonstrated that *CDRT15P1* may facilitate GC's progression and tumor malignancy. Therefore, *CDRT15P1* is not only a promising prognostic biomarker but also a potential molecular therapeutic target for GC.

Ethical statements

This study was conducted in accordance with the Declaration of Helsinki. All data used in this study were obtained from publicly available databases, including TCGA and Gene Expression Omnibus (GEO), and no new human or animal samples were collected. The datasets were fully anonymized prior to analysis; therefore, ethical approval and informed consent were waived.

Author contributions

The authors confirm their contributions to the paper as follows: conceptualization, funding acquisition, supervision: Xia J, Xu F; writing – review and editing: Deng K; investigation: Yang X, Wang F, Liu Q, Yang Y, Yang Z, Yang M, Wang L, Lu S, He Y, Zhao X, Zhang J; writing – original draft: Yang X; software: Wang F; methodology: Liu Q, Yang Y, Yang Z; experiment implementation: Yang X, Du X, Wang X, Wang L; visualization: Yang M; resources: Wang L. All authors reviewed the results and approved the final version of the manuscript.

Data availability

The data analyzed in this study were retrieved from TCGA database (www.cancer.gov/ccg/research/genome-sequencing/tcga), a publicly accessible resource for genomic research.

Acknowledgments

This work was financially supported by National Natural Science Foundation of China (Grant Nos. 82202955 and 82103663), the

Scientific Research Program of Wuxi Health Commission (Grant Nos. Q202329 and Q202223), and Top Talent Support Program for Young and Middle-aged People of Wuxi Health Committee (Grant No. HB2023038).

Conflict of interest

The authors declare that they have no conflict of interest.

Supplementary information accompanies this paper online at: https://doi.org/10.48130/git-0026-0011.

Dates

Received 28 October 2025; Revised 7 April 2026; Accepted 7 May 2026; Published online 31 July 2026

References

[1] Zhang L, Dong Q, Wang Y, Li X, Li C, et al. 2025. Global trends and risk factors in gastric cancer: a comprehensive analysis of the Global Burden of Disease Study 2021 and multi-omics data. *International Journal of Medical Sciences* 22:341–356

[2] Guan WL, He Y, Xu RH. 2023. Gastric cancer treatment: recent progress and future perspectives. *Journal of Hematology & Oncology* 16:57

[3] Yan C, Shan F, Ying X, Li Z. 2023. Global burden prediction of gastric cancer during demographic transition from 2020 to 2040. *Chinese Medical Journal* 136:397–406

[4] Kong W, Wang Z, Wang B. 2023. Unveiling DNA damage repair-based molecular subtypes, tumor microenvironment and pharmacogenomic landscape in gastric cancer. *Frontiers in Genetics* 14:1118889

[5] Zhao Z, Mak TK, Shi Y, Huang H, Huo M, et al. 2023. The DNA damage repair-related lncRNAs signature predicts the prognosis and immunotherapy response in gastric cancer. *Frontiers in Immunology* 14:1117255

[6] Yang E, Chua W, Ng W, Roberts TL. 2021. Peripheral cytokine levels as a prognostic indicator in gastric cancer: a review of existing literature. *Biomedicines* 9:1916

[7] Jiang Y, Wang Y, Chen G, Sun F, Wu Q, et al. 2024. Nicotinamide metabolism face-off between macrophages and fibroblasts manipulates the microenvironment in gastric cancer. *Cell Metabolism* 36:1806–1822.e11

[8] Lo YH, Kolahi KS, Du Y, Chang CY, Krokhotin A, et al. 2021. A CRISPR/Cas9-engineered *ARID1A*-deficient human gastric cancer organoid model reveals essential and nonessential modes of oncogenic transformation. *Cancer Discovery* 11:1562–1581

[9] Zhu Y, Zhou B, Hu X, Ying S, Zhou Q, et al. 2022. LncRNA LINC00942 promotes chemoresistance in gastric cancer by suppressing MSI2 degradation to enhance *c-Myc* mRNA stability. *Clinical and Translational Medicine* 12:e703

[10] The Cancer Genome Atlas Research Network. 2014. Comprehensive molecular characterization of gastric adenocarcinoma. *Nature* 513:202–209

[11] Langfelder P, Horvath S. 2008. WGCNA: an R package for weighted correlation network analysis. *BMC Bioinformatics* 9:559

[12] Zhang B, Horvath S. 2005. A general framework for weighted gene co-expression network analysis. *Statistical Applications in Genetics and Molecular Biology* 4:17

[13] Inoue K, Dewar K, Katsanis N, Reiter LT, Lander ES, et al. 2001. The 1.4-Mb CMT1A duplication/HNPP deletion genomic region reveals unique genome architectural features and provides insights into the recent evolution of new genes. *Genome Research* 11:1018–1033

[14] Yu T, Zhang T, Zhao L, Li K, Li J, et al. 2023. Bioinformatic analysis the expression and clinical significance of CDRT15 in cholangiocarcinoma using TCGA database. *Medicine* 102:e34602

[15] Xu Q, Liu C, Wang H, Li S, Yan H, et al. 2024. Deciphering the impact of aggregated autophagy-related genes TUBA1B and HSP90AA1 on colorectal cancer evolution: a single-cell sequencing study of the tumor microenvironment. *Discover Oncology* 15:431

[16] Khan A, Fornes O, Stigliani A, Gheorghe M, Castro-Mondragon JA, et al. 2018. JASPAR 2018: update of the open-access database of transcription factor binding profiles and its web framework. *Nucleic Acids Research* 46:D260–D266

[17] Karagkouni D, Paraskevopoulou MD, Chatzopoulos S, Vlachos IS, Tastsoglou S, et al. 2018. DIANA-TarBase v8: a decade-long collection of experimentally supported miRNA–gene interactions. *Nucleic Acids Research* 46:D239–D245

[18] Chou CH, Chang NW, Shrestha S, Hsu SD, Lin YL, et al. 2016. miRTarBase 2016: updates to the experimentally validated miRNA-target interactions database. *Nucleic Acids Research* 44:D239–D247

[19] Barbie DA, Tamayo P, Boehm JS, Kim SY, Moody SE, et al. 2009. Systematic RNA interference reveals that oncogenic *KRAS*-driven cancers require TBK1. *Nature* 462:108–112

[20] Rawla P, Barsouk A. 2019. Epidemiology of gastric cancer: global trends, risk factors and prevention. *Gastroenterology Review* 14:26–38

[21] Selcukbiricik F, Buyukunal E, Tural D, Ozguroglu M, Demirelli F, et al. 2013. Clinicopathological features and outcomes of patients with gastric cancer: a single-center experience. *World Journal of Gastroenterology* 19:2154–2161

[22] Wang J, Wu Z, de Groot EM, Challine A, Mohammad NH, et al. 2024. Discontinuation of neoadjuvant therapy does not influence postoperative short-term outcomes in elderly patients (≥ 70 years) with resectable gastric cancer: a population-based study from the dutch upper gastrointestinal cancer audit (DUCA) data. *Gastric Cancer* 27:1114–1123

[23] Arkenau HT, Saggese M, Lemech C. 2012. Advanced gastric cancer: is there enough evidence to call second-line therapy standard? *World Journal of Gastroenterology* 18:6376–6378

[24] Shin HB, An JY, Lee SH, Choi YY, Kim JW, et al. 2017. Is adjuvant chemotherapy necessary in pT1N1 gastric cancer? *BMC Cancer* 17:287

[25] Christodoulidis G, Koumarelas KE, Kouliou MN. 2024. Revolutionizing gastric cancer treatment: the potential of immunotherapy. *World Journal of Gastroenterology* 30:286–289

[26] Zhou J, Ji Q, Li Q. 2021. Resistance to anti-EGFR therapies in metastatic colorectal cancer: underlying mechanisms and reversal strategies. *Journal of Experimental & Clinical Cancer Research* 40:328

[27] Chen DS, Mellman I. 2017. Elements of cancer immunity and the cancer–immune set point. *Nature* 541:321–330

[28] Li YN, Xie B, Zhang Y, He MH, Xing Y, et al. 2023. Advances and key focus areas in gastric cancer immunotherapy: a comprehensive scientometric and clinical trial review (1999–2023). *World Journal of Gastroenterology* 29:5593–5617

[29] Wang Q, Tan W, Zhang Z, Chen Q, Xie Z, et al. 2024. FAT10 induces immune suppression by upregulating PD-L1 expression in hepatocellular carcinoma. *Apoptosis* 29:1529–1545

[30] Zhang J, Dong Y, Yu S, Hu K, Zhang L, et al. 2024. IL-4/IL-4R axis signaling drives resistance to immunotherapy by inducing the upregulation of Fcγ receptor IIB in M2 macrophages. *Cell Death & Disease* 15:500

[31] Wang B, Gu B, Gao L, Ma C, Li X, et al. 2025. SERPINE1 facilitates metastasis in gastric cancer through anoikis resistance and tumor microenvironment remodeling. *Small* 21:2500136

[32] Huang H, Zhou J, Chen H, Li J, Zhang C, et al. 2021. The immunomodulatory effects of endocrine therapy in breast cancer. *Journal of Experimental & Clinical Cancer Research* 40:19

[33] Przemeck SMC, Varro A, Berry D, Steele I, Wang TC, et al. 2008. Hypergastrinemia increases gastric epithelial susceptibility to apoptosis. *Regulatory Peptides* 146:147–156